Density Functional Investigation of Relativistic Effects on the Structure and Reactivity of Tetrahedral Gold Clusters

Himadri Sekhar De,[†] Sailaja Krishnamurty,[‡] and Sourav Pal*[,†]

Theoretical Chemistry Group, Physical Chemistry Division, National Chemical Laboratory, Pune-411008, and Functional Materials Division, Central Electrochemical Research Institute (CECRI), Karaikudi-630 006

Received: January 08, 2009; Revised Manuscript Received: March 01, 2009

The influence of relativistic effects on the structure, vibrational modes, and reactivity of recently discovered tertrahedral gold clusters (Au_{19} and Au_{20}) are investigated using density functional methods. The intramolecular reactivity of the clusters was analyzed using density functional-based reactivity descriptors. The work shows that whereas the structural properties and vibrational modes are considerably affected by the relativistic effects, the reactivity trends based on Fukui function calculation on various atoms within this cluster remain unaffected by the absence or presence of relativistic effects. The reactivity descriptors reveal that the vertex atoms are the most reactive ones in Au_{20} toward a nucleophilic attack. On the other hand, atoms connecting the missing vertex edge with the pyramid base along with the vertex atom are the most reactive for a nucleophilic attack in Au_{19}. The atoms lying at the center of each face are favorable for an electrophilic attack in both cases. Interestingly, the atoms with a missing cap in Au_{19} are highly favorable for electrophilic attack, and Au_{20} has more sites for a favorable nucleophilic attack.

1. Introduction

Gold clusters have been of recent interest because of their rich chemistry and potential applications in the field of molecular electronic devices, catalysis, and as probes for biological diagnostics, and so forth.[1] The most interesting application of the gold nanoclusters is in the area of catalysis.[2,3] Bulk gold is well-known to be chemically inert; the metal does not react with oxygen in air. However, it is now well established that gold clusters from eight atoms or more up to a cluster of 5 nanometers in diameter differ from bulk as they have several surface and corner atoms that have low coordination and hence adopt geometries that are extremely active for catalyzing certain oxidation reactions.[4,5] Since the pioneering reports on the possible application of Au clusters as catalysts, there have been a large amount of experimental and theoretical studies devoted to understand the structural, electronic, catalytic properties, and reactivity of Au_n ($n < 60$) clusters.[6−10] Several interesting findings on Au clusters have been summarized in a recent review on theoretical chemical calculations on gold.[11] These studies have brought out two additional interesting aspects of Au clusters, that is enhanced stability of clusters of particular sizes and, similarly, enhanced catalytic activity of clusters of particular sizes.

A more recent exciting report based on theoretical calculations combined with photoelectron spectroscopy (PES) has established the existence of hollow golden cages for anionic gold clusters with 16−18 atoms with an average cage diameter of 5.5 Å[12]. However, Au_{20} is the most interesting gold cluster reported so far. PES studies have revealed that this anionic Au_{20} cluster has a pyramidal structure (point group, T_d) with each of the three faces and the base representing the (111) surface of the FCC gold. It is reported to have an energy gap of 1.77 eV between the highest occupied molecular orbital (HOMO) and the lowest unoccupied molecular orbital (LUMO). This energy gap is greater than that of C_{60}, thereby indicating that Au_{20} is highly stable and chemically inert.[13] On the other hand, its high surface area and large fraction of corner sites provide ideal surface sites for binding of small molecules like CO, NO_x, and so forth for catalysis. The structure of Au_{19}^- is quite similar to that of Au_{20}^- with one missing corner atom. A more recent experimental vibrational frequency spectroscopic study in combination with the theoretical calculations have shown that neutral Au_{19} and Au_{20} clusters adopt the same symmetry as their anionic counterparts.[14] The high HOMO−LUMO gaps of these two clusters, particularly that of Au_{20} in its neutral, cationic, and anionic forms, has motivated several research groups to work on these clusters, particularly on their structure and stability. The stability of these clusters has been a topic of recent investigation. However, the reactivity of these clusters has not been explored until now. Moreover, most of the theoretical studies to date[15−17] on such clusters have been using the nonrelativistic methods. It is well established by now that gold has very high relativistic effects, much larger than its neighboring elements in the periodic table and larger than any other element with $Z < 100$. Relativistic effects are known to influence the structural aspects of Au clusters[18] as already demonstrated for the case of the small clusters Au_n, (n up to 8) predicted to be nonplanar in the nonrelativistic calculations.[19]

Hence, in this work, the structural and reactivity aspects of these medium-sized Au_{19} and Au_{20} clusters have been analyzed with nonrelativistic and relativistic effects using density functional theory (DFT). The condensed Fukui function (FF) has been used to determine the site reactivity in a system or intramolecular reactivity.[20] The results bring an interesting pattern as to how a single missing cap atom in Au_{20} changes the predominantly nucleophilic attacking sites to predominantly electrophilic attacking favorite sites in Au_{19}. The article is organized as follows. In section 2, we present the brief overview of method used. In section 3, relevant computational details have

* To whom correspondence should be addressed. E-mail: s.pal@ncl.res.in.
[†] National Chemical Laboratory.
[‡] Central Electrochemical Research Institute.

10.1021/jp9001884 CCC: $40.75
Published on Web 04/03/2009

been presented. Section 4 presents results and a discussion on these results.

2. Theoretical Method

The ground-state energy of an atom or a molecule, in DFT, can be expressed in terms of electron density $\rho(r)$ and the function $f(r)$ is defined by

$$f(r) \equiv \left[\frac{d\mu}{d\upsilon(r)}\right] = \left[\frac{\partial \rho}{\partial N}\right]_{\upsilon(r)} \quad (1)$$

f(r) is called the Fukui function (FF) or frontier function for a molecule. The N discontinuity problem of atoms and molecules[21] in eq 1 leads to the introduction[22] of both right- and left-hand-side derivatives at a given number of electrons, N_0 ($=N$)

By the finite difference method, using electron densities of N_0, $N_0 + 1$ and $N_0 - 1$ electron systems, FFs for nucleophilic and electrophilic attack can be defined respectively as,

$$f^+(r) \approx \rho_{N_0+1}(r) - \rho_{N_0}(r) \quad (2a)$$

$$f^-(r) \approx \rho_{N_0}(r) - \rho_{N_0-1}(r) \quad (2b)$$

and for radical attack

$$f^0(r) \approx \frac{1}{2}(\rho_{N_0+1}(r) - \rho_{N_0-1}(r)) \quad (2c)$$

To describe the site reactivity or site selectivity, Yang et al.[23] proposed the condensed FF for an atom k undergoing nucleophilic, electrophilic, or radical attack as

$$f_k^+ \approx q_k^{N_0+1} - q_k^{N_0} \quad (3a)$$

$$f_k^- \approx q_k^{N_0} - q_k^{N_0-1} \quad (3b)$$

$$f_k^0 \approx \frac{1}{2}(q_k^{N_0+1} - q_k^{N_0-1}) \quad (3c)$$

where q_k values are electronic population of the kth atom of a particular species.

To determine the relative nucleophilicity indices, Roy et al. proposed the relative nucleophilicity as[24,25]

$$f_{nu} = f_k^+ / f_k^- \quad (4a)$$

$$f_{el} = f_k^- / f_k^+ \quad (4b)$$

where f_{el} is the relative electrophilicity.

This quantity is quite useful to identify the reactive site at which the reaction takes place. For intramolecular reactivity, $f_{nu/el}$ has the importance in comparing reactivity across the same molecule.

3. Computational Methods

All of the calculations have been performed using *demon.2.2.6* package.[26] The geometries of neutral Au_{19} and Au_{20} were optimized using B88 exchange and Lee, Yang, and Parr correlation functional[27] followed by the calculation of harmonic vibrational frequencies. All of the frequencies were found to be positive, confirming the structure to be a global minima. The basis used for Au is of ECP quality with Stuttgart-Dresden ECP valence basis for nonrelativistic calculations incorporating 19 electrons for treatment and rest electrons being treated as core. For the sake of nonrelativistic calculations, the basis used for calculation is ECP quality with Stuttgart-Dresden ECP for 19 valence electrons treatment. No additional polarization functions have been added. It may be noted that these ECPS are well documented for accurate prediction of structure[14] as well as spectroscopic properties[14,28] of Au clusters. The basis set used for the relativistic calculations is RECP quality with 1997 Stuttgart-Dresden RECP for 19 valence electrons treatment. The A2 auxiliary functions were set to fit the charge density. The convergence of the geometries were based on gradient and displacement criteria with a threshold value of 10^{-5} au and the criteria for convergence of SCF cycles were set to 10^{-9}. The FFs were calculated on the basis of Lowdin SCF population analysis.[29]

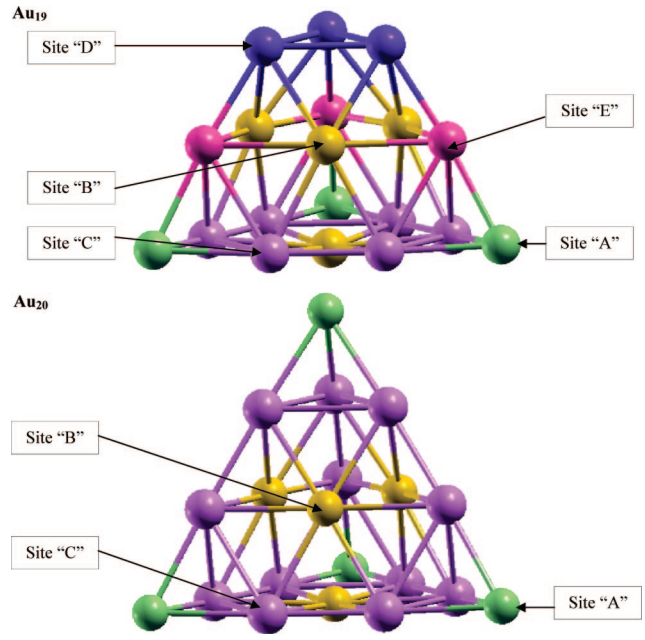

Figure 1. (a) Projection views of the clusters Au_{19} in their ground-state configurations (note, there is no significance to the lines connecting the nuclear positions; these are only an aid for visualization). Geometries were optimized at the ECP/RECP bases with A2 as auxiliary functions. (b) Projection views of the clusters Au_{20} in their ground-state configurations (note, there is no significance to the lines connecting the nuclear positions; these are only an aid for visualization). Geometries were optimized at the ECP/RECP bases with A2 as auxiliary functions

4. Results and Discussion

(a) Structure, Binding Energy, and Vibrational Frequencies. We begin the discussion with a note on the ground-state geometries of Au_{19} and Au_{20} obtained from the relativistic and nonrelativistic calculations. These geometries are shown in parts a and b of Figure 1. Au_{20} has a T_d symmetry with a face centered cubic structure, as shown in part b of Figure 1, whereas Au_{19} has a C_{3v} symmetry. Au_{19} cluster differs from the Au_{20} by a single missing vertex atom of the tetrahedron. This is in good agreement with the earlier reported experimental and theoretical predictions.[14] As seen, both of the clusters are very symmetric, with ordered triangular surfaces stacked over each other. The atoms in both of the clusters are divided into various classes depending upon their symmetry types or environment. Each class of atoms will have a different reactivity. We begin with a classification of atoms in the Au_{19} cluster. This cluster having a C_{3v} point group has five different environments, as shown in part a of Figure 1. They are:

I. Vertex atoms of the pyramid base (site A), coordinated to three atoms.

II. Atoms lying at the center of each face (site B), coordinated to nine atoms.

TABLE 1

(a) Average Interatomic Distances and Bond Angles between Different Sites in Au_{19} and Au_{20}

distance (Å)/bond angles (°)	Au_{19}(nonrelativistic)	Au_{20}(nonrelativistic)	Au_{19}(relativistic)	Au_{20}(relativistic)
A—B	5.269 (5.249)	5.256	4.822	4.819
A—C	3.038	3.058	2.798	2.802
A—E	3.048		2.813	
B—C	3.210	3.127	2.912	2.927
B—D	3.105		2.915	
B—E	3.134		2.927	
C—C	3.020	3.019	2.737	2.745
C—E	3.213		3.075	
D—D	3.158		2.918	
D—E	3.042		2.783	
B—B	3.379	3.365	3.528 (3.437)	3.338
E—B—E	173.6		165.0	
C—B—C	176.7	174.8	169.3	170.4
A—C—C	177.7	177.5	176.0	175.6
C—A—C	64.4	64.1	67.0	67.0
C—C—C	59.9	60.0	60.0	60.0
D—E—A	176.3		174.2	
D—D—D	60.0		60.0	
C—E—A	63.7		66.5	

(b) Charges on Various Sites as Obtained from Lowdin Population Analysis

sites	Au_{19} (nonrelativistic)	Au_{20} (nonrelativistic)	Au_{19} (relativistic)	Au_{20} (relativistic)
A	0.215	0.213	0.228	0.199
B	−0.131	−0.147	−0.223	−0.226
C	−0.044	−0.022	−0.025	0.009
D	0.068		0.102	
E	−0.032		−0.004	

[a] The values in parentheses correspond to case when one of the central atom is in the pyramid base of Au_{19}.

TABLE 2

(A) Reactivity of the Various Sites of $Au_{19}$and Au_{20}

reactivity centers	nonrelativistic Au_{19}, $(f^+)/(f^-)$	nonrelativistic Au_{19}, $(f^-)/(f^+)$	nonrelativistic Au_{20}, $(f^+)/(f^-)$	nonrelativistic Au_{20}, $(f^-)/(f^+)$
A	1.1096	0.9013	2.252	0.502
B	0.9752	1.0295	0.283	3.609
C	0.9888	1.0113	1.083	1.093
D	0.9205	1.0864		
E	1.0098	0.9903		

(b) Reactivity Indices Obtained from Nonrelativistic Calculations

reactivity centers	Au_{19},$(f^+)/(f^-)$	Au_{19}, $(f^-)/(f^+)$	Au_{20}, $(f^+)/(f^-)$	Au_{20},$(f^-)/(f^+)$
A	1.0432	0.9586	1.341	0.746
B	0.9804	1.0216	0.411	2.494
C	0.9735	1.0272	0.996	1.024
D	0.9540	1.0482		
E	1.0681	0.9362		

III. Edge atoms of the pyramid-base (site C), coordinated to six atoms.

IV. Atoms with missing vertex on the top (site D), coordinated to five atoms.

V. Atoms connecting the base of the pyramid and the missing vertex (site E). coordinated to six atoms.

On the other hand, Au_{20}, with T_d symmetry, has only first three classes (A, B, and C). The presence of an additional vertex atom in Au_{20} increases the symmetry of the cluster leading to two less reactive centers within it as compared to Au_{19}. We begin with an analysis of the geometrical parameters of each cluster. Part a of Table 1 shows some important interatomic distances and angles for all of the cases. Part a of Table 2 gives the charges obtained from the Lowdin population analysis on various sites of Au_{19} and Au_{20} for the relativistic and nonrelativistic cases. It is seen from part a of Table 1 that the relativistic effect causes shortening of all the Au—Au bond distances (viz. A—B, A—C, A—E, B—C, B—D, B—E, C—C, C—E, D—D, and D—E) by about 0.2 Å. This shortening of bond lengths is due to the contraction and stabilization of 6s orbitals in contrast to 5d orbitals. It is also interesting to note that most of the Au—Au—Au angles are similar in nonrelativistic and relativistic cases with the exception of E—B—E and C—B—C of Au_{19}. Most of the geometric parameters are also similar between Au_{19} and Au_{20} are similar except for the B—B interatomic distances.

As discussed earlier, the loss of the symmetry in Au_{19} leads to the presence of two additional sites, viz., D and E. The D—D interatomic distances in Au_{19} are longer by about 0.2 Å as compared to C—C distances in the same cluster. On incorporation of relativistic effects, E—B—E and C—B—C angles decrease significantly in Au_{19}. This decrease in the E—B—C and C—B—C angles results in a small curvature within the planes without vertex atoms in Au_{19}, thereby increasing B—B interatomic distances. B—B distances between these planes is 3.5 Å (3.4 Å when one of the atoms is in the pyramid base) as compared to 3.3 Å in Au_{20}.

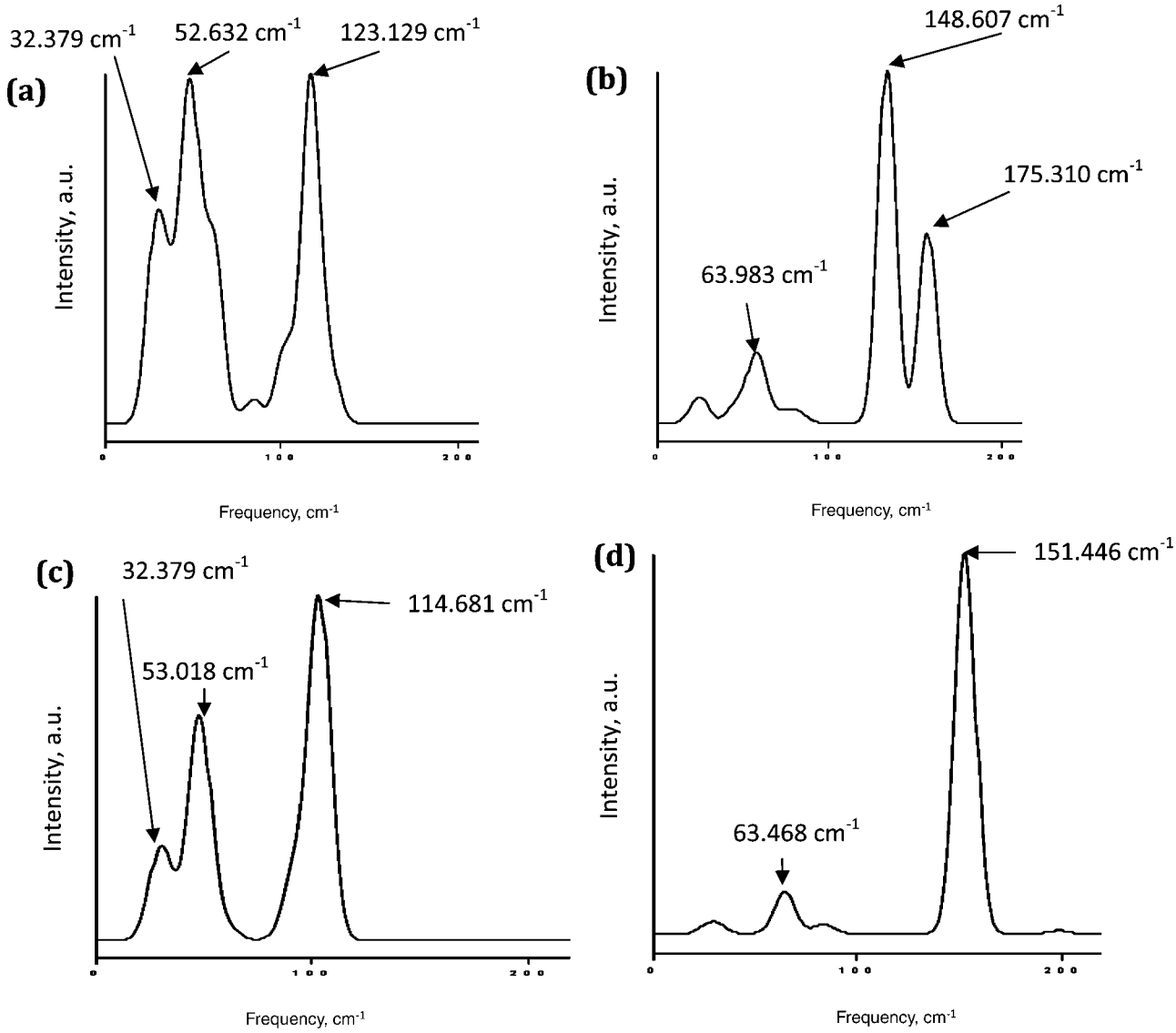

Figure 2. (a) Au_{19} nonrelativistic, (b) Au_{19} relativistic, (c) Au_{20} nonrelativistic, and (d) Au_{20} relativistic. The signals are simulated using Gaussian functions with a half-width value of 6 cm^{-1}. The values were scaled by 1.29.

The distribution of charge across the atoms in both the clusters reveals that the relativistic effects result in greater charge transfer from all of the atoms toward the central atoms. This result in a more negatively charged central atom in both clusters, for example, the average charge on central atoms (site B) of Au_{19} in nonrelativistic calculations is −0.131, which increases to −0.223 when relativistic effects are incorporated. The same in Au_{20} is increased from −0.147 to −0.226 upon incorporation of relativistic effects. This change may be attributed to the following reason: The angles connected with the central atoms (C—B—C and E—B—E) decrease by at the least 4° upon incorporation of relativistic effects. It is by now well-known that a decrease in the Au—Au—Au angle is associated with an increase in the negative charge on the central Au atom at the cost of the edge Au atoms.[30,31] In the present case, it is seen that there is a small charge transfer from sites C, D, and E to the central atom B, leading to a higher negative charge in the B site as a net effect in relativistic cases as seen in part b of Table 1. This results in shorter interatomic distances between the positively charged vertex atoms and negatively charged central atoms (A—B) when the relativistic effects are incorporated (4.82 Å as compared to 5.26 Å in nonrelativistic case). Absence of a vertex atom results in positively charged D sites (0.102) as compared to the C sites, which have a small negative charge (−0.025) on them. This results in larger D—D interatomic distances as compared to the C—C distances as mentioned in the earlier paragraph. This has implications on the reactivity trends as will be discussed in the next sections. In general, it is interesting to note that the central atoms are most negatively charged in both the clusters, whereas the vertex atoms are the positively charged ones. The missing vertex atoms in Au_{19} are the next positively charged centers.

We next analyze the vibrational frequencies of Au_{19} and Au_{20} as obtained from both relativistic and nonrelativistic calculations. IR spectra for Au clusters have been studied using experimental[14,32] and theoretical methods.[33,34] All of the frequencies are positive for Au_{19} and Au_{20} in both relativistic and nonrelativistic methods. In a recent report, Gruene and co-workers have reported the far-infrared (IR) photon dissociation spectrum[14] for neutral Au_{19} and Au_{20} clusters. The experimental IR spectrum of Au_{20} shows a single dominant adsorption around 148 cm^{-1} due to its symmetric structure. The lower symmetry in Au_{19} splits the single adsorption mode into a doubly degenerate vibration (149 cm^{-1}) and a nondegenerate vibration in Au_{19} (168 cm^{-1}). In Figure 2, we present the IR spectrum as obtained from the nonrelativistic calculations and the relativistic calculations. It

is clearly seen that the nonrelativistic calculations do not follow the experimental IR spectra, whereas the relativistic calculations follow the experimental trends. It is noted that the IR spectrum of Au_{19} obtained by relativistic calculations shows a doubly degenerate vibration (e) around 148.6 cm^{-1} and a blue-shifted nondegenerate vibration (a_1) around 174.5 cm^{-1}. Relativistic calculation on Au_{20} shows a triply degenerate vibration (t_2) at 151.4 cm^{-1}. We note that the t_2 vibration in Au_{20} and a_1 vibration in Au_{19} are blue-shifted by 3 and 6 cm^{-1} respectively compared to the experiments and we attribute this difference to the absence of the polarization functions in our calculations. The spectra of both the clusters also show a peak around 63 cm^{-1} corresponding to the rocking mode in the relativistic calculations. On the other hand, nonrelativistic calculations show two dominant peaks in Au_{19} at 52.6 cm^{-1} and 129.1 cm^{-1} as well as Au_{20} at 53.0 cm^{-1} and 114.7 cm^{-1} values, respectively. It is noteworthy that the experimentally reported features are absent in the nonrelativistic calculations, highlighting the importance of the relativistic effects in energy levels of the gold clusters.

(b) Reactivity. Reactivity of these clusters is a matter of great interest because the tetrahedral Au_{20} cluster has been discovered. Whereas charges give a brief insight on the electron redistribution on the cluster, a qualitative understanding on the response of the atom toward an electrophilic or nucleophilic attack using density functional descriptors has been proven to be successful in several earlier studies.[24] Hence, we investigate the trend of relative electrophilicity and nucleophilicity for relativistic and nonrelativistic calculations using FFs for the two studied clusters. The q_k^0 values were calculated for the optimized geometries of neutral Au_{19} and Au_{20} clusters using Lowdin population analysis. q^k_{N-1} and q^k_{N+1} values were obtained by substituting and adding a single electron to the neutral cluster respectively and relaxing the molecular orbitals, while maintaining the same geometry of the neutral cluster. This is a standard procedure used by several groups for calculating the reactivity indices.[35,36] As already discussed, Au_{20} has three types of reactive sites, namely, A, B, and C, whereas Au_{19} has two more additional reactive sites, namely, D and E, owing to the missing vertex atom. In this section, part a of Table 2 gives the relative nucleophilicity and relative electrophilicity of the five sites in Au_{19} and three reactive sites of Au_{20} and part b of Table 2 gives the same for relativistic calculations for the two Au clusters.

We begin with a discussion on the reactivity trends seen for the case of Au_{19}. Interestingly, despite the differences in geometry and vibrational modes seen between relativistic and nonrelativistic calculations, the reactivity descriptors obtained from these two calculations predict similar reactivity order among atoms. It is seen that site A corresponding to the vertex atoms in Au_{19} and sites E are more favorable sites for a nucleophilic attack as compared to the other three sites. Atoms with the missing vertex (site D) are least favorable sites for nucleophilic attack. For the case of an electrophilic attack, sites B (central atoms), C, and D are more favorable. Coming to the case of Au_{20}, the vertex atoms (site A) are most favorable for a nuecleophilic attack as in case of Au_{19}. The central atoms, that is sites B, are the most favorable ones for electrophilic attack.

We also note that the relative nucleophilicity of the vertex atom is much higher in case of Au_{20} as compared to Au_{19}, in which, along with the vertex atoms, sites E show a higher affinity toward nucleophilic reagents. The central atoms, that is the atoms at reactive sites B, are most reactive for electrophilic attack in both the clusters. Apart from that, the sites with missing vertex C are the additional counterparts for electrophilic attack. Interestingly, in both the cases we find that incorporation of relativistic effect does not show a marked change in the trend of the reactivity of various reactive centers in both of the Au clusters. We finally note that Au_{19} has more sites favorable for an electrophilic attack, and Au_{20} has more sites for an favorable nucleophilic attack. Thus, it is interesting to note how a single missing cap atom changes a predominatly nucloephilic attack favorable Au_{20} to a predominantly electrophlic attack favorable Au_{19}.

5. Conclusions

The above discussion brings out clearly how the relativistic effects are important for a good description of geometry and vibrational frequencies. However, the density functional-based reactivity descriptors bring out the same trend in reactivity, irrespective of the presence or absence of these effects, emphasizing the robustness of these descriptors. These descriptors predict relative nucleophilicity of the vertex atom to be higher in case of Au_{20} as compared to Au_{19}. It is seen that relativistic effects have no influence on catalytic activity of the Au clusters. The most reactive atoms in Au_{19} correspond to the atoms that are not capped by any vertex atom. The reactivity descriptors also predict that the vertex atoms are the most reactive ones in Au_{20} toward a nucleophilic attack, whereas atoms connecting the missing vertex edge with the pyramid base along with the vertex atom are the most reactive ones for nucleophilic attack in Au_{19}. The atoms lying at the center of each face are favorable for an electrophilic attack in both the cases. The atoms with a missing cap in Au_{19} are highly favorable for electrophilic attack. The present work clearly brings out how the presence of all of the vertex atoms in Au_{20} results in more sites for a favorable nucleophilic attack.

Acknowledgment. The authors acknowledge the Center of excellence in Computational Chemistry at NCL, Pune for the calculations presented. H.D. acknowledges Council of Scientific and Industrial Research (CSIR) for a fellowship. S.P. acknowledges J.C. Bose fellowship of DST and SSB grant of CSIR towards fulfillment of the work.

References and Notes

(1) *Gold. Progress in Chemistry, Biochemistry and Technology*; Schmidbaur, H., ed.; Wiley: Chichester, 1999; p 894.
(2) Teles, J. H.; Brode, S.; Chabanas, M. *Angew. Chem.* **1998**, *37*, 1415.
(3) Hashmi, A. S. K. *Gold Bull.* **2003**, *36*, 3.
(4) Haruta, M. *Gold Bull.* **2004**, *37*, 27.
(5) Haruta, M.; Daté, M. *Appl. Catal., A* **2001**, *222*, 427.
(6) Pyykko, P. *Angew. Chem., Int. Ed.* **2004**, *43*, 4412.
(7) Pyykkö, P. *Angew. Chem., Int. Ed.* **2002**, *41*, 3573.
(8) Haruta, M. *Catal. Today* **1997**, *36*, 153.
(9) Chrétien, S.; Metiu, H. *J. Chem. Phys.* **2007**, *127*, 084704.
(10) Lemire, C.; Meyer, R.; Shaikhutdinov, Sh.K.; Freund, H.-J. *Surf. Sci.* **2004**, *552*, 27.
(11) Pykko, P. *Chem. Rev.* **2008**, *37*, 1967.
(12) Bulusu, S.; Li, X.; Wang, L. S.; Zeng, X. C. *Proc. Natl. Acad. Sci. U.S.A.* **2006**, *103*, 8326.
(13) Li, J.; Li, X.; Zhai, H. J.; Wang, L. S. *Science* **2003**, *299*, 864.
(14) Gruene, P.; Rayner, D. M.; Redlich, B.; van der Meer, A. F. G.; Lyon, J. T.; Meiger, G.; Fielicke, A. *Science* **2008**, *321*, 674.
(15) Wang, J.; Wang, G.; Zhao, J. *Phys. Rev. B* **2002**, *66*, 035418.
(16) Garzón, I. L.; Michaelian, K.; Beltrán, M. R.; Posada-Amarillas, A.; Ordejón, P.; Artacho, E.; Sánchez-Portal, D.; Soler, J. M. *Phys. Rev. Lett.* **1998**, *81*, 1600.
(17) Michaelian, K.; Rendón, N.; Garzón, I. L. *Phys. Rev. B* **1999**, *60*, 2000.
(18) (a) Haberlen, O. D.; Chung, S. C.; Stener, M.; Rosch, N. *J. Chem. Phys.* **1997**, *106*, 5189. (b) Bowmaker, G. A.; Schmidbaur, H.; Kruger, S.; Rosch, N. *Inorg. Chem.* **1997**, *36*, 1754.
(19) Hakkinen, H.; Moseler, M.; Landman, U. *Phys. Rev. Lett.* **2002**, *89*, 033401.

(20) Parr, R. G.; Yang, W. *J. Am. Chem. Soc.* **1984**, *106*, 4049. (b) Yang, W.; Parr, R. G. *Proc. Natl. Acad. Sci. U.S.A* **1985**, *82*, 6723.

(21) Perdew, J. P.; Parr, R. G.; Levy, M.; Balduz, J. L., Jr. *Phys. Rev. Lett.* **1982**, *49*, 1691. (b) Zhang, Y.; Yang, W. *Theor. Chem. Acc.* **2000**, *103*, 346.

(22) Parr, R. G.; Yang, W. *J. Am. Chem. Soc.* **1984**, *106*, 4049.

(23) Yang, W.; Mortier, W. *J. Am. Chem. Soc.* **1986**, *108*, 5708.

(24) Roy, R. K.; Krishnamurti, S.; Geerlings, P.; Pal, S. *J. Phys. Chem. A* **1998**, *102*, 3746.

(25) Roy, R. K.; Proft, F.; Geerlings, P. *J. Phys. Chem. A* **1998**, *102*, 7035.

(26) Fischer, G.; Goursot, A.; Coq, B.; Delahay, G.; Pal, S. *ChemPhysChem* **2006**, *7*, 1795.

(27) Perdew, J. P.; Burke, K.; Erzenhof, M. *Phys. Rev. Lett.* **1996**, *77*, 3865.

(28) Schwerdtfeger, P.; Dolg, M.; Schwarz, W. H. E.; Bowmaker, G. A.; Boyd, P. D. W. *J. Chem. Phys.* **1989**, *91*, 1762.

(29) Mulliken, R. S. J. *Chem. Phys.* **1955**, *23*, 1833.

(30) Joshi, A. M.; Tucker, M. H.; Delgass, W. N.; Thomson, K. T. *J. Chem. Phys.* **2006**, *125*, 194707.

(31) Shafai, G. S.; Shetty, S.; Krishnamurty, S.; Shah, V.; Kanhere, D. G. *J. Chem. Phys.* **2007**, *126*, 014704.

(32) Pichugina, D. A.; Kuz'menko, N. E.; Shestakov, A. F. *Proc. SPIE—Int. Soc. Opt. Eng.* **2006**, *6580*, 658003.

(33) Kryachko, E. S.; Remacle, F. *Int. J. Quantum Chem.* **2007**, *107*, 2922.

(34) Molina, B.; Soto, J. R.; Calles, A. *Revisra Mexicana de Fisica* **2008**, *54*, 314.

(35) Chattaraj, P. K. *J. Phys. Chem. A* **2001**, *105* (2), 511–513.

(36) Kar, R.; Chandrakumar, K. R. S.; Pal, S. *J. Phys. Chem. A* **2007**, *111*, 375–383.

JP9001884